THE JOURNAL OF PHYSICAL CHEMISTRY Letters

Cite This: J. Phys. Chem. Lett. 2018, 9, 36−42

Letter

pubs.acs.org/JPCL

From Solvent-Free to Dilute Electrolytes: Essential Components for a Continuum Theory

Nir Gavish,[†] Doron Elad,[†] and Arik Yochelis*[,‡,¶]

[†]Department of Mathematics, Technion - IIT, Haifa 3200003, Israel

[‡]Department of Solar Energy and Environmental Physics, Swiss Institute for Dryland Environmental and Energy Research, Blaustein Institutes for Desert Research, Ben-Gurion University of the Negev, Sede Boqer Campus, Midreshet Ben-Gurion 8499000, Israel

[¶]Department of Physics, Ben-Gurion University of the Negev, Be'er Sheva 8410501, Israel

Supporting Information

ABSTRACT: The increasing number of experimental observations on highly concentrated electrolytes and ionic liquids show qualitative features that are distinct from dilute or moderately concentrated electrolytes, such as self-assembly, multiple-time relaxation, and underscreening, which all impact the emergence of fluid/solid interfaces, and the transport in these systems. Because these phenomena are not captured by existing mean-field models of electrolytes, there is a paramount need for a continuum framework for highly concentrated electrolytes and ionic liquid mixtures. In this work, we present a self-consistent spatiotemporal framework for a ternary composition that comprises ions and solvent employing a free energy that consists of short- and long-range interactions, along with an energy dissipation mechanism obtained by Onsager's relations. We show that the model can describe multiple bulk and interfacial morphologies at steady-state. Thus, the dynamic processes in the emergence of distinct morphologies become equally as important as the interactions that are specified by the free energy. The model equations not only provide insights into transport mechanisms beyond the Stokes−Einstein−Smoluchowski relations but also enable qualitative recovery of three distinct regions in the full range of the nonmonotonic electrical screening length that has been recently observed in experiments in which organic solvent is used to dilute ionic liquids.

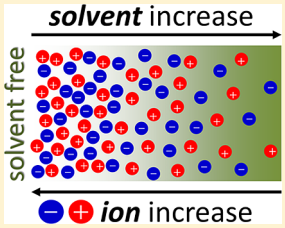

Concentrated electrolytes are being examined for a broad range of applications[1−4] and specifically for energy-related devices, examples of which include dye-sensitized solar cells, fuel cells, batteries, and supercapacitors.[5−7] Optimizing the design of these devices requires mechanistic understanding of the spatial ionic arrangement and charge transport in electrolytes. Although the physicochemical aspects of electrolyte solutions have been extensively studied, a series of recent experimental and computational results[8−19] exposes knowledge gaps in the underlying basic science.[3,16,20−24] A robust spatiotemporal framework is thus required to advance industrial applications of highly concentrated electrolytes, e.g., fuel cells ∼1 M (mol/liter) and batteries ∼10 M.

Theoretical formulation of electrolytes' spatiotemporal behavior goes back to the 1890s with the formulation of the continuum mean-field Poisson−Nernst−Planck (PNP) equations.[25,26] The PNP model describes ions as isolated point charges that obey drift-diffusion transport under an electric potential and is a well-established theory for dilute electrolytes.[27] This description is valid for electrolytes with concentrations typically below ∼0.01M but is oversimplified for concentrated electrolytes where, for example, the finite size of the ions should be taken into account.[28,29] Consequently, extensive studies during the past centennial have led to major modifications of the mean-field approach in order to tackle steady state electrical double layers (EDLs) or electrokinetic properties; see representative reviews[20,21,24,30] and references therein. Among the broad family of modified PNP and Poisson−Boltzmann (PB) models, we highlight for our purposes the steric-PNP (SPNP) approach that has been employed for studying permeability and selectivity in ion channels,[31] where ion concentrations exceed 10 M. This approach accounts for Lennard-Jones-type interactions between the ions, which are similar to the interactions employed in molecular dynamics (MD) simulations.

Theoretically (i.e., excluding the ion-pairing question[22]), the upper limit of "concentrated electrolytes" corresponds to molten salts, i.e., solvent-free electrolytes which at about room temperature, are also being referred to as ionic liquids (ILs).[5,6] Besides their multiple applications, ILs, both with and without dilution, may exhibit several intriguing properties: (i) multiple time scales,[17,32] (ii) self-assembly,[33−35] and (iii) nonmonotonic variation (exhibiting qualitatively three distinct regions) of EDL with concentration,[15,36] a.k.a., the phenomenon of *underscreening*. These phenomenologies clearly indicate that, despite the vast progress in concentrated electrolytes, a framework that unifies all these phenomena is still missing.[24]

Here we present a dynamical and thermodynamically consistent, unified continuum framework, based on SPNP and Onsager's relations, for *ternary* media (i.e, solutions of anions, cations, and solvent). Our goal is to present a theoretical framework by outlining the essential features that

Received: November 16, 2017
Accepted: December 8, 2017
Published: December 8, 2017

DOI: 10.1021/acs.jpclett.7b03048
J. Phys. Chem. Lett. 2018, 9, 36−42

are designed to pave the road toward a realistic description of concentrated electrolytes: (i) explicit densities of electrically positive, negative, and neutral subsets (aqueous or organic carriers), (ii) finite-size (steric) effects, and (iii) selective energy dissipation to reflect mass transport. While we follow the SPNP formulation, the starting point originates with ILs[37,38] and introduces explicitly the solvent density. Our testing of the qualitative model results, appears to capture and relate, in broad parameter regimes, the aforementioned phenomena to effects of polarization[3] and self-assembly,[23] and to explain the origins of nonmonotonic electrical screening length variation.[15,36] In particular, at high concentrations, the system is expected to form different morphologies, in both the EDL and bulk region, that are strongly dictated by spatiotemporal instabilities that drive the self-assembly process in the bulk, as indeed observed in models for pure ILs[37,40] and charged diblock copolymers.[41]

Model Equations for a Ternary Composition. In general, PNP-type models consider the solvent as an effective background medium. This assumption, however, breaks down in the high-concentration limit, e.g., in ILs. Therefore, we derive a ternary model by considering first model equations for asymmetric pure ILs[38] and introducing the solvent as an explicit field. Specifically, we assume a monovalent electrolyte composed of cations (p), anions (n), and solvent (s), identified by their the molar concentrations in terms of the partial volume that is occupied by each species

$$\frac{p}{p_{\max}} + \frac{n}{n_{\max}} + \frac{s}{s_{\max}} = 1 \tag{1}$$

where $p_{\max}$, $n_{\max}$, and $s_{\max}$ are the maximal concentrations (packing densities) of the cations, anions, and solvent molecules, respectively. Following Onsager's framework, cf. ref 37, the transport equations are given by

$$\frac{\partial}{\partial t}\begin{pmatrix} p \\ n \\ s \end{pmatrix} = \nabla\cdot\begin{bmatrix} p_{\max}-p & -p & -p \\ -n & n_{\max}-n & -n \\ -s & -s & s_{\max}-s \end{bmatrix}\begin{pmatrix} p\mathbf{J}^p \\ n\mathbf{J}^n \\ s\mathbf{J}^s \end{pmatrix} \tag{2a}$$

and the Coulombic interactions obey the standard Poisson's equation

$$\nabla(\epsilon\nabla\phi) = q(n-p) \tag{2b}$$

where q is the elementary charge and ϵ is the dielectric permittivity (assumed here to be constant). The respective fluxes are obtained from the variation (functional derivative) of the free energy

$$\mathbf{J}^p = \frac{\mu_B}{\bar{c}_{\max}}\nabla\frac{\delta\mathcal{F}}{\delta p} \qquad \mathbf{J}^n = \frac{\mu_B}{\bar{c}_{\max}}\nabla\frac{\delta\mathcal{F}}{\delta n} \qquad \mathbf{J}^s = \frac{\mu_B}{\bar{c}_{\max}}\nabla\frac{\delta\mathcal{F}}{\delta s}$$

where

$$\mathcal{F} = \int_\Omega \mathrm{d}\mathbf{x}\, \overbrace{k_BT\left[p\ln\frac{p}{\bar{c}} + n\ln\frac{n}{\bar{c}} + s\ln\frac{s}{\bar{s}}\right]}^{\text{entropy}} + \overbrace{\left[q(p-n)\phi - \frac{\epsilon}{2}|\nabla\phi|^2\right]}^{\text{electrostatic}} + \underbrace{\bar{c}_{\max}\left[\frac{\beta}{n_{\max}p_{\max}}np + \mathcal{E}_0\frac{\kappa^2}{2}\left(\left|\nabla\frac{p}{p_{\max}}\right|^2 + \left|\nabla\frac{n}{n_{\max}}\right|^2\right)\right]}_{\text{local approximation of Lennard-Jones interactions}}, \tag{3}$$

Ω is the considered physical domain, μ_B is the mobility coefficient, β is the interaction parameter (a.k.a., Flory parameter in the context of mixing energy for polymers) for the anion/cation mixture, $\mathcal{E}_0\kappa^2$ is the gradient energy coefficient with units of energy for the former and units of length for the latter, $\bar{c}$ is the average concentration of ionic species, and $\bar{s}$ is the average concentration of solvent molecules

$$\bar{c} := \frac{1}{|\Omega|}\int_\Omega p\,\mathrm{d}\mathbf{x} = \frac{1}{|\Omega|}\int_\Omega n\,\mathrm{d}\mathbf{x} \qquad \bar{s} := \frac{1}{|\Omega|}\int_\Omega s\,\mathrm{d}\mathbf{x}$$

Notably, global charge neutrality and the equal valence of the anions and cations ensure that the average concentration of cations equals the average concentration of anions. This implies, together with the electrolyte incompressibility assumption (eq 1), that the maximal average concentration (achieved when $\bar{s} = 0$), equals the harmonic average of $p_{\max}$ and $n_{\max}$

$$\frac{1}{\bar{c}_{\max}} = \frac{1}{p_{\max}} + \frac{1}{n_{\max}}$$

Model Interpretation. To reveal the physical properties of the key parameters of the model equations (eq 2), we rewrite the equations in their dimensionless form (see the SI for details) and for simplicity present only the equation for cations while the equation for anions is given in the SI

$$\frac{\partial p}{\partial t} = \nabla\cdot(\mathbf{J}^p_{\mathrm{PNP}} + c\mathbf{J}^p_1 + c^2\mathbf{J}^p_2 + c^3\mathbf{J}^p_3) \tag{4}$$

where

$$\mathbf{J}^p_{\mathrm{PNP}} = \underbrace{\nabla p + p\nabla\phi}_{\text{drift-diffusion}} \tag{5a}$$

$$\mathbf{J}^p_1 = \underbrace{\frac{2\Upsilon}{1+\gamma}p\nabla(p+n)}_{\text{solvent entropy}} - \underbrace{p\mathbf{J}^p_{\mathrm{PNP}}}_{\text{saturated mobility}} - \underbrace{p\mathbf{J}^n_{\mathrm{PNP}} + \frac{\chi}{1+\gamma}p\nabla n}_{\text{interdiffusion}} \tag{5b}$$

$$\mathbf{J}^p_2 = \underbrace{-\frac{1}{1+\gamma}p[\sigma\nabla^3 p + \chi\nabla(pn)]}_{\text{steric effects}} \tag{5c}$$

$$\mathbf{J}^p_3 = \underbrace{\frac{\sigma}{(1+\gamma)}p(p\nabla^3 p + n\nabla^3 n)}_{\text{steric effects}} \tag{5d}$$

The normalized global ion concentration $0 \le c \le 1$ is a key parameter that relates the ions to the solvent via $(1-c)s = 1 - c(p+n)$. In particular, c is scaled such that $c = 0$ corresponds to the vanishing concentration of ions (dilute limit), while $c = 1$ corresponds to the absence of solvent (IL); powers of c describe equal contributions of terms in the equations and do not imply a perturbative expansion. Here, σ is a measure of the ratio between relative strength of short-range steric and long-range Coloumbic interactions, χ is also related to steric interactions rescaled to the ambient temperature, γ is the size ratio between cations and anions, and Υ is the complementary size asymmetry between the solvent and ions. In particular, $\Upsilon \approx 1$ for solvent molecules whose size is similar to the size of the ions (e.g., DMF), and $\Upsilon \gg 1$ for solvent molecules that are much smaller than the ions (e.g., water).

It is instructive to consider the ionic flux term-by-term to reveal the impact of different mechanisms on electrolyte behavior as concentration is varied. For the simplicity of

DOI: 10.1021/acs.jpclett.7b03048
J. Phys. Chem. Lett. 2018, 9, 36−42

presentation, we do so by choosing $\mathbf{J}^p$ while components of $\mathbf{J}^n$ are given in the SI. At the dilute limit, $c \ll 1$, steric effects are negligible, i.e., $\mathbf{J}^p \approx \mathbf{J}^p_{\mathrm{PNP}}$. Therefore, eq 4 reduces to the classical PNP theory. Similarly, in the solvent-free limit, $c \simeq 1$, the model (eq 4) reduces to the model for pure ILs[38] that was shown to exhibit multiple time scale dynamics in the context of transient currents.[37] To understand how electrolyte behavior varies at intermediate concentrations, let us first consider terms of $\mathbf{J}^p_1$, that is, c contributions. The first term in $\mathbf{J}^p_1$ is related to solvent entropy, and reflects the solvent tendency to diffuse to the regions of high ionic concentration (or low solvent concentration). This effect becomes dominant when $\Upsilon \gg 1$, i.e., when solvent molecules are significantly smaller than the ions, because the entropy per volume of many small particles is larger than the entropy of a fewer larger particles. The second term corresponds to saturated mobility, which gradually diminishes the transport of cations to cation-rich regions. This term prevents the formation of regions with a local concentration of constitutes beyond their packing density. The final two terms correspond to interdiffusion (a.k.a., mutual- or cross-diffusion) where species movement results in opposite gradients of the electrochemical potentials of the anions and cations. Here, the motion reflects the increase/decrease in the local anion or cation concentrations, which is partially balanced by a decrease/increase of the total charge concentration, as well as by change in solvent concentration. We emphasize that these mechanisms are not introduced "by hand" to the model; they are results of the explicit inclusion of solvent, and, to a lesser extent, the assumption of electrolyte incompressibility. Indeed, while Nernst−Planck dynamics (leading to Stokes−Einstein−Smoluchowski relations) arise from a random walk description of isolated ions in an effective medium, the inclusion of solvent implies that species are not isolated. The movement of a cation, for example, involves pushing aside solvent molecules and possibly anions in its path, and movement of solvent to the void left behind.

At higher orders, the combined effect of all terms can be comprehended in one space dimension (1D) by neglecting the boundary conditions and considering the case $\gamma = \Upsilon = 1$. In this case, substituting eq 2b into eq 5b, the flux takes the form of high-order corrections for the drift $\mathbf{J}^p_1 = p\nabla^3\phi$, and thus, $\nabla\cdot\mathbf{J}^p_1$ gives rise to a fourth-order derivative of the electric potential that addresses short-range correlations[42−45] (we note that originally the high-order operator was introduced phenomenologically for ILs by Bazant−Storey−Kornyshev[44] through a displacement field in eq 2b). In the next section, we show that, under appropriate conditions, these short-range interactions give rise to self-assembled nanopatterns near charged interfaces and/or in the bulk.

Analysis: Nonmonotonic Screening Length. The broad family of generalized PNP models describes electrolyte solutions with a spatially uniform bulk.[20,30,46] Equation 4 gives rise to a richer picture of bulk and interfacial behavior, which is consistent with the picture arising in recent experimental and numerical studies.[21,23,33,35,47−49] Indeed, using spatial linearization methods (see the SI for details), we map the qualitatively distinct bulk and interfacial behaviors and the corresponding regions in the parameter space spanned by ion size asymmetry γ and normalized concentration c; see Figure 1. The results have been obtained in one space dimension ($\nabla \to \partial_x$) and with no-flux boundary conditions (inert electrodes) for ions and Dirichlet boundary conditions for the potential (constant applied voltage): $J^p(x = \pm L/2) = 0$ and $\phi(x = \pm L/2) = \pm V/2$, where L is the physical domain size and V is the applied voltage.

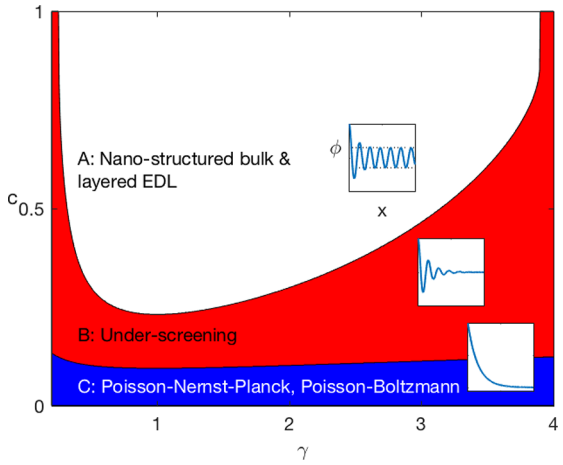

Figure 1. Parameter space spanned by the concentration (c) and ion size asymmetry (γ), showing the transitions from a monotonic EDL as described by the PNP or PB model (dark shaded region), the region of the oscillatory EDL giving rise to underscreening (light shaded region), and the region of self-assembled bulk. Parameters: $\Upsilon = 4$, $\sigma = 10$, $\chi = 30$.

Region A describes the emergent self-assembly of the bulk nanostructure, i.e., a spatially oscillatory profile throughout the whole domain; see the top inset in Figure 1. Here, the region is obtained numerically from the onset of the finite wavenumber instability.[38] This region is characterized by highly concentrated electrolyte with weak ion size asymmetries (typical size ratios of roughly 1:2 or 1:3). Indeed, the first observations of self-assembly were for protic ILs with short alkyl groups,[33] although the phenomenon of self-assembly has been observed in many other compositions.[23]

Region C corresponds to a homogeneous bulk with a monotone EDL structure, as shown in the bottom inset of Figure 1. This region is characterized by low enough concentrations so that steric effects are perturbative, and the model reduces to the PNP theory of dilute electrolytes (or PB theory if steady states are of interest). The latter also demonstrates that sufficiently diluted ILs, either by solvent[47] or possibly by formation of ion pairs,[19,50] can behave as dilute electrolytes.

The intermediate Region B describes a homogeneous bulk with an oscillatory potential and charge density profiles near a charged interface (a.k.a, a spatially decaying oscillatory EDL), as shown in the middle inset. The onset of this region is computed using spatial dynamics methods,[51,52] as detailed in the SI. Notably, these decaying oscillations have also been referred to as overscreening.[44,53]

The three regions in Figure 1 imply that as an IL or concentrated electrolyte solution with relatively weak ion-size asymmetry ($\gamma \approx 1$) is diluted it exhibits a transition from nanostructured bulk and a layered EDL at high ionic concentration (i.e., at region A) to a layered EDL with homogeneous bulk (region B), and finally, at low concentrations, to a monotonic EDL structure. Insets A−C in Figure 2 present steady-state solutions of eq 4 with parameters corresponding to the IL, $[C_4C_1Pyrr][NTf_2]$, diluted with propylene carbonate ($C_4H_6O_3$). Indeed, a transition from layered to monotonic EDL has been observed using high-energy X-ray reflectivity[47] and in situ AFM[48] within the range

DOI: 10.1021/acs.jpclett.7b03048
J. Phys. Chem. Lett. 2018, 9, 36−42

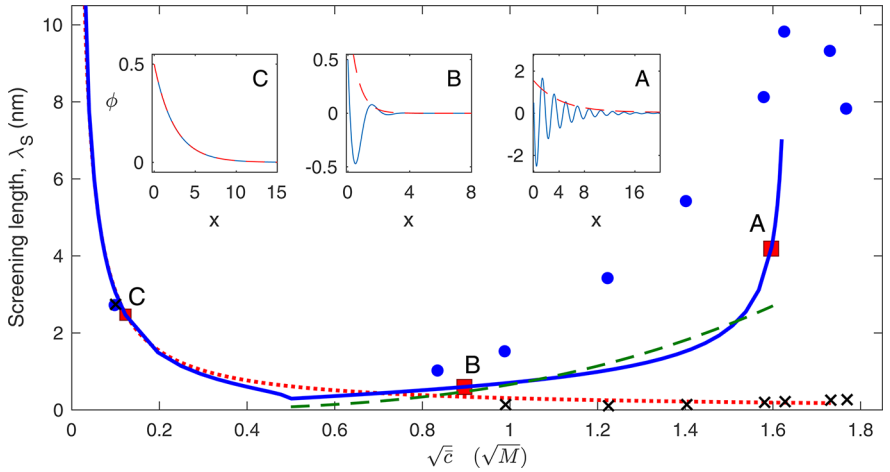

Figure 2. Screening length as a function of concentration $\bar{c}$ for the IL, $[C_4C_1Pyrr][NTf_2]$, diluted with propylene carbonate ($C_4H_6O_3$); the concentration is scaled according to the dependence of the Debye length. Experimental data from ref 15 (●) is superimposed with the computed screening length (solid curve) for dimensional parameters that correspond to this IL; see the SI for details. For comparison, we also plotted the monotonically decaying Debye−Hückel approximation, λ_D (dotted red curve), the hypernetted chain correction[9] (×), and the curve $2/3\bar{c}^{3/2}$ (dashed curve) to allow comparison with the recently presented scaling argument.[55] Insets A−C present spatial profiles of the electric potential ϕ at different concentrations (solid curve, ■) and the exponential envelop (dashed curve) that is computed by the real part of the spatial eigenvalues (eq 6), which is being used as a measure for the screening length. Dimensionless parameters: $\gamma = 1$, $\Upsilon = 1$, $\chi = 28$, $\sigma = 35$, $V = 1$, and $L = 200$.

of parameters considered here. The molecular origin for the transition from monotonic to spatially oscillatory EDL (a.k.a., the Kirkwood line) has been outlined using hypernetted chain[9] and mean spherical[54] approximations already in the early 1990s. However, as has been outlined by Smith et al.,[15] and also demonstrated in Figure 2, there are significant differences in comparison with empirical measurements. Moreover, the transition from region B to region A appears to be unexplored by available mean-field models. In what follows, we show that this transition is associated with an unexpected mechanistic decrease in the screening length with increasing concentration;[15,36] see region $\sqrt{\bar{c}} \gtrsim 1.6\sqrt{M}$ in Figure 2.

To examine the transition from region C to B, we use the size-symmetric $\gamma = 1$ case to derive analytic relations that are otherwise obtained numerically, as shown in the SI. Above the monotonic to spatially oscillatory decay onset, the spatial decay is insufficiently described by the PB approach, and instead, the screening length is better related to the envelope of the decaying oscillations.[9] In other words, the screening length is related to the spatial scale at which the bulk electroneutrality is violated[51,52] (the tail of oscillation amplitudes) rather than to the electrolyte behavior in the vicinity of the solid surface. Indeed, in Figure 2A, we observe that the envelope of the oscillatory tail (dashed curve) otherwise describes the screening length well, but does not describe the electrolyte behavior near the boundary, i.e., in the first two left spatial oscillations near $x = 0$.

Following the redefinition of the screening length with the scale at which electroneutrality is violated, the formal computation involves linearization in space about a uniform bulk $p \equiv p_0(c)$ and $n \equiv n_0(c)$ corresponding to the normalized concentration c

$$p = p_0 + \delta_p e^{\mu x} \qquad n = n_0 + \delta_n e^{\mu x} \qquad \phi = \delta_\phi e^{\mu x}$$

where $|\delta_p|$, $|\delta_n|$, and $|\delta_\phi| \ll 1$ are the respective eigenvector components at the onset. In this case, the screening length is the reciprocal of the real part of the spatial eigenvalues, $\lambda_S \approx \mathrm{Re}(1/\mu)$, that are associated with the eigenvalue problem; see the SI for details. Particularly, in the size-symmetric case ($\gamma = \Upsilon = 1$), explicit expressions of these eigenvalues can be derived, where, of the several eigenvalues obtained, the relevant ones are given by

$$\mu_\pm^2 = \frac{4 - \chi c}{2c^2\sigma}\left[1 \pm \sqrt{1 - 16\sigma c^2/(4 - \chi c)^2}\,\right] \tag{6}$$

Figure 2 presents the computed screening length as a function of concentration for parameters corresponding to a specific IL, $[C_4C_1Pyrr][NTf_2]$, diluted with propylene carbonate. In accordance with experimental observations, at low concentrations where the EDL structure monotonically decreases, the screening length becomes identical to the Debye length. As the electrolyte concentration is increased above the Kirkwood point, $c_c = 4(\chi - 4\sigma)/(\chi^2 - 16\sigma) \simeq 0.077$, the envelope tail length increases and exceeds the Debye length. Switching to dimensional units, the transition is at $0.48\sqrt{M}$, which corresponds to the minimum in the IL screening length (Figure 2). Accordingly, the increase in the concentration leads to the phenomenon of underscreening.[15,36] As introduced by Lee et al.,[55] in a regime of concentration beyond the Kirkwood point, we observe that the screening length roughly scales as $c^{3/2}$ with respect to the Debye screening length.

While the transition from regions C and B can be formulated using near-equilibrium methods,[21,30,57] it is not true for the transition from region B to A. Here, the significance of the spatiotemporal approach (eq 2) in the context of screening length structure becomes fundamental as the temporal bulk instability is approached, i.e., region A. At the instability onset, the real part of the relevant eigenvalues $\mathrm{Re}(\mu_\pm) \to 0$ and hence the screening length in a pure 1D system should extend to infinity, $\lambda_S \to \infty$. This onset is in fact an analogue of the (temporal) finite wavenumber instability bifurcation point, as discussed in more detailed by Gavish et al.[37,41] However, in reality, the system is higher than 1D representation, so that secondary time-dependent zigzag instabilities[56] of the bulk self-assembly become dominant in an appropriate parameter regime.[37,41] In this case, spatial oscillations of the screening

DOI: 10.1021/acs.jpclett.7b03048
J. Phys. Chem. Lett. 2018, 9, 36−42

length are destroyed and the screening length effectively follows instead a decreasing spatially oscillatory profile, cf. ref 40. Indeed, the second decay in screening length has been reported at high concentrations; cf. refs 15 and 36 and Figure 2. The asymptotic methods applied in regions B and C cannot treat this phenomenon, and spatiotemporal framework is therefore required for a mechanistic explanation of this behavior.[24,30,57,58]

Consequently, as summarized in Figure 2, the above results qualitatively capture the experimental observation of all three regions of the nonmonotonic screening length dependence on concentration, as well as reducing to the PNP theory at low concentrations.[15] We have also tested the consistency of our results with parameters that correspond to aqueous NaCl and have again obtained a good qualitative comparison, as shown in Figure 1 in the SI.

In this work, we have introduced a spatiotemporal thermodynamically consistent continuum mean-field framework for electrolytes that ranges from solvent-free to dilute concentrations with explicit treatment of the solvent medium and finite size (steric) effects of both ion and solvent components. These two components introduce, by consistency, an additional transport mechanism of interdiffusion and bulk nanostructuring by self-assembly. We conjecture that these are the essential features that mean-field models for electrolytes should aim to include, in order to provide a comprehensive description at a wide range of concentrations, including the approach to a solvent-free case. While it is true that other approaches (such as, a repulsive Yukawa potential, the hard sphere potential in Rosenfeld's density functional theory of fluids, and asymptotic PB-type models) may be efficient in some specific cases,[19,30,45,49,59,60] the existing approaches cannot capture the screening length behavior at a full range of concentrations. We therefore chose to focus on the screening length to emphasize the importance of including the energy dissipation and self-assembly features, and specifically on secondary transverse instabilities that explain the experimentally observed second decay at high concentrations.[15,36] Notably, the advantage of the spatiotemporal framework is apparent in cases where understanding of temporal and/or morphological bulk effects is required, such as in self-assembly. A detailed analysis of secondary instabilities is beyond the scope of this Letter and will be presented elsewhere.

The advantage of the framework we developed is not only its consistency with different previous continuum approaches,[9,28,31,37,39,40,58,61] but also its amenability to potential extensions to account for additional effects, e.g., ion−solvent interactions, ion-pairing,[19,22,62−64] or other electrostatic corrections.[65] These extensions should be advanced via quantitative comparisons with experimental observations, beyond the qualitative trends depicted in Figure 2. Consequently, we expect that the current spatiotemporal framework will stimulate experiments that combine temporal methods with structural analysis;[66] for example, comparisons to transport properties via multiple time scale relaxations that have been already shown to be present for pure ILs due to interdiffusion and saturated mobility[37] (not addressed here in detail) as systematic (for comparison purposes) experimental data is presently limited at large.[17,32]

■ ASSOCIATED CONTENT

Supporting Information

The Supporting Information is available free of charge on the ACS Publications website at DOI: 10.1021/acs.jpclett.7b03048.

Additional details of the dimensional form, the dimensionless equation for anions, spatial analysis and distinct regions, screening length and comparison, parameters for diluted ionic liquid, and parameters and comparison with NaCl aqueous electrolyte (PDF)

■ AUTHOR INFORMATION

Corresponding Author

*E-mail: yochelis@bgu.ac.il.

ORCID

Arik Yochelis: 0000-0002-1516-0766

Notes

The authors declare no competing financial interest.

■ ACKNOWLEDGMENTS

We thank Sariel Bier for commenting on the manuscript. This research was done in the framework of the Grand Technion Energy Program (GTEP) and of the BGU Energy Initiative Program and supported by the Adelis Foundation for renewable energy research. N.G. acknowledges support from the Technion VPR fund and from EU Marie−Curie CIG Grant 2018620.

■ REFERENCES

(1) Niedermeyer, H.; Hallett, J.; Villar-Garcia, I.; Hunt, P.; Welton, T. Mixtures of ionic liquids. *Chem. Soc. Rev.* **2012**, *41*, 7780−7802.

(2) Perkin, S. Ionic liquids in confined geometries. *Phys. Chem. Chem. Phys.* **2012**, *14*, 5052−5062.

(3) Fedorov, M. V.; Kornyshev, A. A. Ionic Liquids at Electrified Interfaces. *Chem. Rev.* **2014**, *114*, 2978−3036.

(4) Zhang, S.; Zhang, J.; Zhang, Y.; Deng, Y. Nanoconfined Ionic Liquids. *Chem. Rev.* **2017**, *117*, 6755−6833.

(5) Armand, M.; Endres, F.; MacFarlane, D.; Ohno, H.; Scrosati, B. Ionic-liquid materials for the electrochemical challenges of the future. *Nat. Mater.* **2009**, *8*, 621−629.

(6) Wishart, J. Energy applications of ionic liquids. *Energy Environ. Sci.* **2009**, *2*, 956−961.

(7) Salanne, M. Ionic Liquids for Supercapacitor Applications. *Top. Curr. Chem.* **2017**, *375*, 1−25.

(8) Israelachvili, J. N.; Adams, G. E. Measurement of forces between two mica surfaces in aqueous electrolyte solutions in the range 0−100 nm. *J. Chem. Soc., Faraday Trans. 1* **1978**, *74*, 975−1001.

(9) Attard, P. Asymptotic analysis of primitive model electrolytes and the electrical double layer. *Phys. Rev. E* **1993**, *48*, 3604.

(10) Leote de Carvalho, R.; Evans, R. The decay of correlations in ionic fluids. *Mol. Phys.* **1994**, *83*, 619−654.

(11) Biesheuvel, P.; Van Soestbergen, M. Counterion volume effects in mixed electrical double layers. *J. Colloid Interface Sci.* **2007**, *316*, 490−499.

(12) Mansoori, G.; Carnahan, N. F.; Starling, K.; Leland, T., Jr Equilibrium thermodynamic properties of the mixture of hard spheres. *J. Chem. Phys.* **1971**, *54*, 1523−1525.

(13) Kirchner, B.; Malberg, F.; Firaha, D. S.; Hollóczki, O. Ion pairing in ionic liquids. *J. Phys.: Condens. Matter* **2015**, *27*, 463002.

(14) Lee, A. A.; Kondrat, S.; Vella, D.; Goriely, A. Dynamics of ion transport in ionic liquids. *Phys. Rev. Lett.* **2015**, *115*, 106101.

(15) Smith, A. M.; Lee, A. A.; Perkin, S. The electrostatic screening length in concentrated electrolytes increases with concentration. *J. Phys. Chem. Lett.* **2016**, *7*, 2157−2163.

(16) Yochelis, A.; Singh, M.; Visoly-Fisher, I. Coupling Bulk and Near-Electrode Interfacial Nanostructuring in Ionic Liquids. *Chem. Mater.* **2015**, *27*, 4169−4179.

(17) Makino, S.; Kitazumi, Y.; Nishi, N.; Kakiuchi, T. Charging current probing of the slow relaxation of the ionic liquid double layer at the Pt electrode. *Electrochem. Commun.* **2011**, *13*, 1365−1368.

DOI: 10.1021/acs.jpclett.7b03048
J. Phys. Chem. Lett. 2018, 9, 36−42

(18) Limmer, D. T. Interfacial ordering and accompanying divergent capacitance at ionic liquid-metal interfaces. *Phys. Rev. Lett.* **2015**, *115*, 256102.
(19) Adar, R. M.; Markovich, T.; Andelman, D. Bjerrum pairs in ionic solutions: A Poisson-Boltzmann approach. *J. Chem. Phys.* **2017**, *146*, 194904.
(20) Bazant, M. Z.; Kilic, M. S.; Storey, B. D.; Ajdari, A. Towards an understanding of induced-charge electrokinetics at large applied voltages in concentrated solutions. *Adv. Colloid Interface Sci.* **2009**, *152*, 48−88.
(21) Iglič, A.; Drobne, D.; Kralj-Iglič, V. *Nanostructures in Biological Systems: Theory and Applications*; CRC Press, 2015.
(22) Lee, A.; Vella, D.; Perkin, S.; Goriely, A. Are Room-temperature Ionic Liquids Dilute Electrolytes? *J. Phys. Chem. Lett.* **2015**, *6*, 159−163.
(23) Hayes, R.; Warr, G. G.; Atkin, R. Structure and nanostructure in ionic liquids. *Chem. Rev.* **2015**, *115*, 6357−6426.
(24) Goodwin, Z. A.; Kornyshev, A. A. Underscreening, overscreening and double-layer capacitance. *Electrochem. Commun.* **2017**, *82*, 129−133.
(25) Nernst, W. Die elektromotorische wirksamkeit der jonen. *Z. Phys. Chem.* **1889**, *4*, 129−181.
(26) Planck, M. Ueber die erregung von electricität und wärme in electrolyten. *Ann. Phys.* **1890**, *275*, 161−186.
(27) Bard, A. J.; Faulkner, *Electrochemical Methods: Fundamentals and Applications*, 2nd ed.; Wiley: New York, 2002.
(28) Bikerman, J. Structure and capacity of electrical double layer. *The London, Edinburgh, and Dublin Philosophical Magazine and Journal of Science* **1942**, *33*, 384.
(29) Booth, F. The dielectric constant of water and the saturation effect. *J. Chem. Phys.* **1951**, *19*, 391−394.
(30) Varela, L. M.; GarcıÌa, M.; Mosquera, V. Exact mean-field theory of ionic solutions: non-Debye screening. *Phys. Rep.* **2003**, *382*, 1−111.
(31) Horng, T.-L.; Lin, T.-C.; Liu, C.; Eisenberg, B. PNP equations with steric effects: a model of ion flow through channels. *J. Phys. Chem. B* **2012**, *116*, 11422−11441.
(32) Camci, M.; Aydogan, P.; Ulgut, B.; Kocabas, C.; Suzer, S. XPS enables visualization of electrode potential screening in an ionic liquid medium with temporal-and lateral-resolution. *Phys. Chem. Chem. Phys.* **2016**, *18*, 28434−28440.
(33) Atkin, R.; Warr, G. The smallest amphiphiles: Nanostructure in protic room-temperature ionic liquids with short alkyl groups. *J. Phys. Chem. B* **2008**, *112*, 4164−4166.
(34) Lo Celso, F.; Yoshida, Y.; Castiglione, F.; Ferro, M.; Mele, A.; Jafta, C.; Triolo, A.; Russina, O. Direct experimental observation of mesoscopic fluorous domains in fluorinated room temperature ionic liquids. *Phys. Chem. Chem. Phys.* **2017**, *19*, 13101−13110.
(35) Pontoni, D.; Haddad, J.; Di Michiel, M.; Deutsch, M. Self-segregated nanostructure in room temperature ionic liquids. *Soft Matter* **2017**, *13*, 6947−6955.
(36) Smith, A. M.; Lee, A. A.; Perkin, S. Switching the structural force in ionic liquid-solvent mixtures by varying composition. *Phys. Rev. Lett.* **2017**, *118*, 096002.
(37) Gavish, N.; Yochelis, A. Theory of phase separation and polarization for pure ionic liquids. *J. Phys. Chem. Lett.* **2016**, *7*, 1121−1126.
(38) Bier, S.; Gavish, N.; Uecker, H.; Yochelis, A. From bulk self-assembly to electrical diffuse layer in a continuum approach for ionic liquids: The impact of anion and cation size asymmetry. *Phys. Rev. E* **2017**, *95*, 060201.
(39) Psaltis, S.; Farrell, T. W. Comparing charge transport predictions for a ternary electrolyte using the Maxwell−Stefan and Nernst−Planck equations. *J. Electrochem. Soc.* **2011**, *158*, A33−A42.
(40) Lazaridis, K.; Wickham, L.; Voulgarakis, N. Fluctuating hydrodynamics for ionic liquids. *Phys. Lett. A* **2017**, *381*, 1431−1438.
(41) Gavish, N.; Versano, I.; Yochelis, A. Spatially localized self-assembly driven by electrically charged phase separation. *SIAM J. Appl. Dyn. Syst.* **2017**, *16*, 1946−1968.
(42) Santangelo, C. D. Computing counterion densities at intermediate coupling. *Phys. Rev. E* **2006**, *73*, 041512.
(43) Liu, J.-L.; Eisenberg, B. Correlated ions in a calcium channel model: a Poisson−Fermi theory. *J. Phys. Chem. B* **2013**, *117*, 12051−12058.
(44) Bazant, M. Z.; Storey, B. D.; Kornyshev, A. A. Double layer in ionic liquids: Overscreening versus crowding. *Phys. Rev. Lett.* **2011**, *106*, 46102.
(45) Blossey, R.; Maggs, A. C.; Podgornik, R. Structural interactions in ionic liquids linked to higher-order Poisson-Boltzmann equations. *Phys. Rev. E* **2017**, *95*, 060602.
(46) Gavish, N.; Promislow, K. On the structure of Generalized Poisson−Boltzmann equations. *Eur. J. Appl. Math.* **2016**, *27*, 667−685.
(47) Mezger, M.; Roth, R.; Schröder, H.; Reichert, P.; Pontoni, D.; Reichert, H. Solid-liquid interfaces of ionic liquid solutions - Interfacial layering and bulk correlations. *J. Chem. Phys.* **2015**, *142*, 164707.
(48) Cui, T.; Lahiri, A.; Carstens, T.; Borisenko, N.; Pulletikurthi, G.; Kuhl, C.; Endres, F. Influence of Water on the Electrified Ionic Liquid/Solid Interface: A Direct Observation of the Transition from a Multilayered Structure to a Double-Layer Structure. *J. Phys. Chem. C* **2016**, *120*, 9341−9349.
(49) Maggs, A.; Podgornik, R. General theory of asymmetric steric interactions in electrostatic double layers. *Soft Matter* **2016**, *12*, 1219−1229.
(50) Gebbie, M.; Valtiner, M.; Banquy, X.; Henderson, W.; Israelachvili, J. Experimental observations demonstrate that ionic liquids form both bound (Stern) and diffuse electric double layers. *Proc. Natl. Acad. Sci. U. S. A.* **2013**, *110*, E4122.
(51) Yochelis, A. Transition from non-monotonic to monotonic electrical diffuse layers: Impact of confinement on ionic liquids. *Phys. Chem. Chem. Phys.* **2014**, *16*, 2836−2841.
(52) Yochelis, A. Spatial structure of electrical diffuse layers in highly concentrated electrolytes: A modified poisson-nernst-planck approach. *J. Phys. Chem. C* **2014**, *118*, 5716−5724.
(53) Levin, Y. Electrostatic correlations: from plasma to biology. *Rep. Prog. Phys.* **2002**, *65*, 1577.
(54) Buzzeo, M.; Evans, R.; Compton, R. Non-haloaluminate room-temperature ionic liquids in electrochemistry - A Review. *ChemPhysChem* **2004**, *5*, 1106−1120.
(55) Lee, A. A.; Perez-Martinez, C.; Smith, A. M.; Perkin, S. Scaling Analysis of the Screening Length in Concentrated Electrolytes. *Phys. Rev. Lett.* **2017**, *119*, 026002.
(56) Cross, M.; Hohenberg, P. Pattern formation outside of equilibrium. *Rev. Mod. Phys.* **1993**, *65*, 851−1112.
(57) Attard, P. Electrolytes and the electric double layer. *Adv. Chem. Phys.* **1996**, *92*, 1−160.
(58) Storey, B.; Bazant, M. Effects of electrostatic correlations on electrokinetic phenomena. *Phys. Rev. E* **2012**, *86*, 056303.
(59) Ben-Yaakov, D.; Andelman, D.; Podgornik, R.; Harries, D. Ion-specific hydration effects: Extending the Poisson-Boltzmann theory. *Curr. Opin. Colloid Interface Sci.* **2011**, *16*, 542−550.
(60) Giera, B.; Henson, N.; Kober, E. M.; Shell, M. S.; Squires, T. M. Electric double-layer structure in primitive model electrolytes: comparing molecular dynamics with local-density approximations. *Langmuir* **2015**, *31*, 3553−3562.
(61) Borukhov, I.; Andelman, D.; Orland, H. Steric effects in electrolytes: A modified Poisson-Boltzmann equation. *Phys. Rev. Lett.* **1997**, *79*, 435−438.
(62) Marcus, Y.; Hefter, G. Ion pairing. *Chem. Rev.* **2006**, *106*, 4585−4621.
(63) Merlet, C.; Madden, P. A.; Salanne, M. Internal mobilities and diffusion in an ionic liquid mixture. *Phys. Chem. Chem. Phys.* **2010**, *12*, 14109−14114.
(64) Hollóczki, O.; Malberg, F.; Welton, T.; Kirchner, B. On the origin of ionicity in ionic liquids. Ion pairing versus charge transfer. *Phys. Chem. Chem. Phys.* **2014**, *16*, 16880−16890.
(65) Schlumpberger, S.; Bazant, M. Z. Simple Theory of Ionic Activity in Concentrated Electrolytes. *arXiv:1709.03106 [physics.chem-ph]* **2017**.

DOI: 10.1021/acs.jpclett.7b03048
J. Phys. Chem. Lett. 2018, 9, 36−42

(66) Reichert, P.; Kjær, K. S.; Brandt van Driel, T.; Mars, J.; Ochsmann, J. W.; Pontoni, D.; Deutsch, M.; Nielsen, M. M.; Mezger, M. Molecular Scale Structure and Dynamics at an Ionic Liquid/Electrode Interface. *Faraday Discuss.* **2018**, DOI: 10.1039/C7FD00171A.

DOI: 10.1021/acs.jpclett.7b03048
J. Phys. Chem. Lett. 2018, 9, 36−42